archives
of thermodynamics
Vol. **44**(2023), No. 2, 87–114
DOI: 10.24425/ather.2023.146560

Mixed convection heat transfer of a nanofluid in a square ventilated cavity separated horizontally by a porous layer and discrete heat source

HAMDI MESSAOUD[a*]
SAHI ADEL[a]
OURRAD OUERDIA[b]

[a] Université de Bejaia, Laboratoire de Physique Théorique, Faculté de Technologie, Algeria

[b] Université de Bejaia, Laboratoire de Physique Théorique, Faculté des Sciences Exactes, Algeria

Abstract Laminar mixed convection heat transfer in a vented square cavity separated by a porous layer filled with different nanofluids (Fe_3O_4, Cu, Ag and Al_2O_3) has been investigated numerically. The governing equations of mixed convection flow for a Newtonian nanofluid are assumed to be two-dimensional, steady and laminar. These equations are solved numerically by using the finite volume technique. The effects of significant parameters such as the Reynolds number ($10 \leq Re \leq 1000$), Grashof number ($10^3 \leq Gr \leq 10^6$), nanoparticle volume fraction ($0.1 \leq \phi \leq 0.6$), porous layer thickness ($0 \leq \gamma \leq 1$) and porous layer position ($0.1 \leq \delta \leq 0.9$) are studied. Numerical simulation details are visualized in terms of streamline, isotherm contours, and average Nusselt number along the heated source. It has been shown that variations in Reynolds and Darcy numbers have an impact on the flow pattern and heat transfer within a cavity. For higher Reynolds ($Re > 100$), Grashof ($Gr > 10^5$) numbers and nanoparticles volume fractions the heat transfer rate is enhanced and it is optimal at lower values of Darcy number ($Da = 10^{-5}$). In addition, it is noticed that the porous layer thickness and location have a significant effect on the control of the heat transfer rate inside the cavity. Furthermore, it is worth noticing that Ag nanoparticles presented the largest heated transfer rate compared to other nanoparticles.

Keywords: Mixed convection; Vented cavity; Porous layer; Finite volume method

*Corresponding Author. Email: messaoud.hamdi@univ-bejaia.dz

Nomenclature

a	–	thickness of porous layer, m
b	–	position of porous layer, m
C_p	–	heat capacity, J/kg K
Da	–	Darcy number
F	–	the inertia coefficient
h	–	length of heated source, m
g	–	gravitational acceleration, m/s^2
Gr	–	Grashof number
K	–	permeability of porous layer
L	–	cavity length and height, m
Nu	–	Nusselt number
P	–	dimensionless pressure
Pr	–	Prandtl number
Ra	–	Rayleigh number
Re	–	Reynolds number
T	–	temperature, K
U, V	–	dimensionless velocity components
u, v	–	velocity components in x, y directions, m/s
w	–	size of inlet and outlet port
X, Y	–	dimensionless coordinates
x, y	–	Cartesians coordinates, m

Greek symbols

α	–	thermal diffusivity, m^2/s
β	–	thermal expansion coefficient at constant pressure, 1/K
δ	–	dimensionless position of porous layer
γ	–	dimensionless thickness of porous layer
ε	–	porosity of porous layer
λ	–	thermal conductivity, W/m K
μ	–	dynamic viscosity, Pa s
ρ	–	density of fluid, kg/m^3
ϕ	–	nanoparticles volume fraction
θ	–	dimensionless temperature

Subscripts and superscripts

eff	–	effective
f	–	fluid
h, c	–	hot and cold temperature
i, j	–	x–y components
nf	–	nanofluid
p	–	porous medium
s	–	solid

1 Introduction

The study of mixed convection in an open or vented cavity induced by combined effects of mechanical inflow and buoyancy force has so far been a fundamental research area and requires comprehensive analysis to understand the physics of resulting flow and heat transfer. This is frequently encountered in engineering applications such as cooling of electronic and microelectronic equipment, heating and air conditioning, solar energy collection, nuclear reactors and heat exchangers [1–7].

The vented cavity is one of the most studied geometries in heat transfer, due to its application in electronic equipment cooling. Different configurations have been studied. Mehrizi *et al.* [8] used the lattice Boltzmann method (LBM) to investigate the effect of nanoparticles suspension on the mixed convection in a square cavity with inlet and outlet ports and a hot obstacle in the vented cavity. It was found that the heat transfer rate enhanced with the increasing nanoparticles volume concentration. Ismael and Jasim [9] investigated fluid-structure interaction in mixed convection inside a vented cavity having two inlet and outlet openings. They reported that a flexible fin enhances the Nusselt number better than a rigid fin. Benzema *et al.* [10] used the thermodynamic second law to study magnetohydrodynamic (MHD) mixed convection heat transfer in a vented irregular cavity filled with a hybrid nanofluid. Their results showed that adding nanoparticles to water improves heat transfer but increases total entropy generation. Selimefendigil and Oztop [11] examined magnetohydrodynamics forced convection in a layered U-shaped vented cavity with a porous layer under the wall corrugation impact. It was found that the flow field and heat transfer are impacted by the Reynolds number, Hartmann number and Darcy number. Ataei-Dadavi *et al.* [12] conducted an experimental study of mixed convection in a vented, differentially side-heated cubical cavity filled with a porous medium. The results showed that there are three different flow and heat transfer regimes depending on the Richardson number. Dhahad *et al.* [13] studied numerically mixed convection in a vertically vented cavity using the spectral element method. Moayedi [14] investigated the heat transfer of Cu-water nanofluid in laminar convection around double rotating cylinders in a vented cavity with different inlet and outlet ports. They reported that the mean Nusselt number increases with the nanofluid volume fraction and rotational Reynolds number. Velkennedy *et al.* [15] have studied convective flow in a ventilated cavity having two outlets and one inlet with cold partitions using the finite difference method. They showed that

the presence of cold partitions modifies the flow structure inside a ventilated cavity. Recently, Jamshed *et al.* [16] conducted a numerical analysis of MHD mixed convection in a ventilated porous cavity with a heated elliptic inner cylinder filled with nanofluid. They demonstrated that the average Nusselt number increases when the Richardson number and porosity ratio increase.

Currently, mixed convection in nanofluids has been the subject of several theoretical, experimental and especially numerical studies. Among them; Benos and Sarris [17] presented an analytical study of MHD natural convection of nanofluid in a shallow cavity. Arani *et al.* [18] have used the finite volume method to solve numerically the natural convection in a square cavity with a heated horizontal plate containing a nanofluid. Results showed that the mean Nusselt number increases with the increasing nanoparticles volume fraction and decreases as the heated plate location varies from the top to bottom of the cavity. Selimefendigil and Öztop [19] studied mixed convection in a lid-driven cavity filled with ferrofluid in the presence of two rotating cylinders. They observed that flow patterns and thermal transport are affected by the Reynolds number and magnetic dipole strength variations. Rabbi *et al.* [20] studied MHD mixed convection in a ferrofluid filled lid-driven cavity for different heater configurations. They observed that the higher Richardson number enhances the heat transfer rate, although the higher Hartmann number decreases the heat transfer rate. Elshehabey *et al.* [21] investigated numerically natural convection with a nonlinear Boussinesq approximation in an inclined and partially open cavity. Jakeer *et al.* [22] studied magneto-hybrid nanofluid flow in a lid-driven porous cavity with an inside heated square obstacle. Recently, Wang and Xu [23] investigated mixed convection in an inclined lid-driven cavity filled with a hybrid nanofluid. They indicated that hybrid nanofluid is superior to traditional heat transfer fluids for heat transfer enhancement. Jayaprakash *et al.* [24] suggested a mathematical model to illustrate the flow and radiative heat transfer of a hybrid nanofluid over a curved stretching sheet. Their results showed that the heat transfer enhanced with the increasing radiation parameter and Biot number. Dutta *et al.* [25] performed a study of mixed convection in a ventilated cavity filled with viscoplastic hybrid nanofluid and with a mounted heated solid obstacle. It is observed from their analysis that the heat transfer rate enhanced with the inclusion of Cu nanoparticles in Al_2O_3-viscoplastic fluid.

Convection heat transfer within an enclosure filled with a porous medium has become important owing to its benefits in diversified applications in various areas. Numerous studies have explored the phenomenon. Neild and

Bejan [26] presented a board literature review about convection in porous media. Balla *et al.* [27] investigated the flow and heat transfer of the MHD boundary layer in a nanofluid-filled inclined porous square cavity. Their results are obtained for different values of the Rayleigh number, inclination angle, magnetic field and nanofluid volume fraction. The effect of MHD convection of nanofluid in a porous enclosure with sinusoidal heating was investigated by Malik and Nayak [28]. They found that the heat transfer rate and entropy generation depend on the Grashof, Hartmann and Darcy numbers. Sheremet *et al.* [29] studied mixed convection in a square porous cavity filled with a water-based nanofluid under suction/injection zones effects. It has been found that an increase in Rayleigh and Darcy numbers leads to flow acceleration near the heated wall. Abu-Hamdeh *et al.* [30] investigated the impact of various parameters in a lid-driven cavity filled with porous media having a one-side opening in the presence of heat generation. They found that the heat transfer rate rises and decreases as the heater length and Grashof number increase, respectively. Maboud *et al.* [31] considered the unsteady MHD incompressible Casson fluid flow in porous media. Kumar *et al.* [32] examined the non-Newtonian hybrid nanofluid flow through a porous moving rotating disk. Kashyap and Dass [33] investigated numerically the influence of inclination of the cavity on mixed convection in a double-sided lid-driven cavity with a hot porous square blockage. The results reveal that the inclination significantly impacts the heat transfer rate and entropy production. Alsedais *et al.* [34] examined the influence of radiation and heat generation on MHD mixed convection of a nanofluid in an inclined undulating porous cavity containing an obstacle. Choudhary and Ray [35] worked on a porous-corrugated enclosure containing a discrete heat source. They found that different parameters (Rayleigh, Darcy and Hartmann numbers) have a significant effect on flow behaviour. Nammi *et al.* [36] have explored numerically unsteady natural convection heat transfer within a square-shaped porous cavity with four heated cylinders. Recently, Kumar *et al.* [37] used original mathematical models to evaluate convective flow dynamics of viscous dissipative heat and mass transfer in a doubly stratified fluid saturated porous enclosure.

Convection heat transfer with a superposed fluid and porous layers confined in an enclosure (partly layered enclosure) have been studied early because of their great mathematical and practical interest, such as in fuel cells, solidification, and many other systems [38–41]. Aly *et al.* [42] studied the effects of wavy nanofluid/porous interface on mixed convection and entropy generations of Cu-water nanofluid. Under the influence of a uniform

inclined magnetic field, Astanina *et al.* [43] explored natural convection in an open trapezoidal cavity including a porous layer and a ferrofluid layer. Their result showed that growth of the porous layer height leads to a reduction of the heat transfer rate. Selimefendigil and Öztop [44] studied the curved porous layer impact on forced convection heat transfer and entropy generation in a vented cavity filled with hybrid nanofluid under inclined magnetic field effects by using the finite volume method. Gibanov *et al.* [45] examined MHD mixed convection in a lid-driven cavity partially filled with a porous medium saturated with a ferrofluid. It is found that the magnetic field inclination angle and porous layer height influence greatly the heat transfer enhancement and fluid flow intensification. Al-Srayyih *et al.* [46] investigated natural convection inside a superposed enclosure filled with composite porous-hybrid nanofluid layers. They observed that the heat transfer rate in a hybrid nanofluid is higher than within pure fluid. Al-Zamily [47] carried out a numerical analysis of natural convection and entropy generation in a cavity filled with multi-layers of porous medium and nanofluid with heat generation. They showed that the Nusselt number depends on the heat source position. Moria [48] studied improvements of porous layers in natural convection of an L-shape enclosure, with different parameters considered. Recently, Alsabery *et al.* [49] provided a numerical investigation of two-phase flow and heat transfer for hybrid nanofluid in a wavy enclosure partially filled with a porous medium. They indicated that hybrid nanofluid is better for heat transfer enhancement compared to simple nanofluid. It's worthy of note that there are other interesting papers on this subject with various other applications [50–53].

Motivated by the above-mentioned research, the present study focuses on numerical simulations of mixed convection in a ventilated square cavity filled with different nanofluids containing a horizontal porous layer with a heated source. It should be noted that this investigation is driven by the need to understand the heat transfer mechanisms in heat exchangers by analyzing the performance of the insertion of a porous layer associated with the addition of nanoparticles to the base fluid.

2 Mathematical formulation

We consider steady laminar, two-dimensional, mixed convection inside a vented square cavity filled with nanofluid having a horizontal porous layer with thickness a ($\gamma = a/L$) and position b ($\delta = b/L$). A schematic of

the problem under investigation and the coordinate system are shown in Fig. 1.

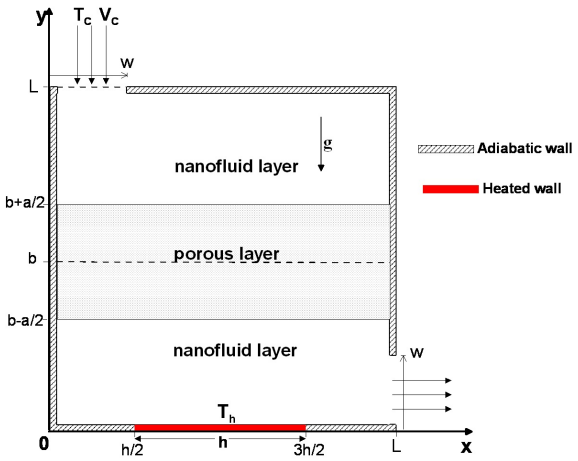

Figure 1: Schematic description of the physical system.

The cavity side length and height are denoted by L. The inflow opening is located on the left of the upper wall and the outflow opening of the cavity is fixed at the right wall bottom. The inlet port size is the same as that of the outlet port, which is equal to $w = 0.2L$. It is assumed that incoming flow is at a constant velocity (V_c) and low temperature (T_c). A heat source is located at the middle of the bottom wall with a higher temperature T_h and at a length denoted by $h = 0.5L$, and all other walls are thermally insulated. Basic fluid (water) and different spherical nanoparticles are in thermal equilibrium and their properties are presented in Table 1.

Table 1: Physical properties of the based fluid and nanoparticles [45, 49]

Physical property	Units	Base fluid (water)	Fe_3O_4	Cu	Ag	Al_2O_3
C_p	J/kg K	4179	670	385	235	765
ρ	kg/m^3	997.1	5200	8933	10500	3970
λ	W/m K	0.613	6	401	429	40
$\beta \times 10^{-5}$	K^{-1}	21.0	1.3	1.67	1.89	0.85
μ	Pa s	0.001003	–	–	–	–

The Forchheimer–Brinkman-extended Darcy model and Boussinesq approximation are applicable. The domain boundaries are impermeable, while

the interface between clear fluid and porous medium is permeable. The porous medium is saturated with a nanofluid that is in local thermodynamic equilibrium with the solid matrix and is assumed to be homogeneous and isotropic. Nanofluid thermophysical properties are constant, except for the density variation, which is determined based on the Boussinesq approximation. Governing conservation equations for laminar and steady Newtonian fluid flow with consideration of the above-mentioned assumptions can be written in the following form:

For the nanofluid layer:

Continuity

$$\frac{\partial u}{\partial x}+\frac{\partial v}{\partial y}=0\,. \tag{1}$$

Momentum

$$v\frac{\partial u}{\partial y}=-\frac{1}{\rho_{nf}}\frac{\partial p}{\partial x}+\frac{\mu_{nf}}{\rho_{nf}}\left(\frac{\partial^2 u}{\partial x^2}+\frac{\partial^2 u}{\partial y^2}\right), \tag{2}$$

$$v\frac{\partial u}{\partial y}=-\frac{1}{\rho_{nf}}\frac{\partial p}{\partial x}+\frac{\mu_{nf}}{\rho_{nf}}\left(\frac{\partial^2 u}{\partial x^2}+\frac{\partial^2 u}{\partial y^2}\right). \tag{3}$$

Energy

$$u\frac{\partial T}{\partial x}+v\frac{\partial T}{\partial y}=\alpha_{nf}\left(\frac{\partial^2 T}{\partial x^2}+\frac{\partial^2 T}{\partial y^2}\right). \tag{4}$$

For the porous layer:

Continuity

$$\frac{\partial u}{\partial x}+\frac{\partial v}{\partial y}=0\,. \tag{5}$$

Momentum

$$\begin{aligned} u\frac{\partial u}{\partial x}+v\frac{\partial u}{\partial y}=&-\frac{\varepsilon^2}{\rho_{nf}}\frac{\partial p}{\partial x}+\frac{\varepsilon\mu_{nf}}{\rho_{nf}}\left(\frac{\partial^2 u}{\partial x^2}+\frac{\partial^2 u}{\partial y^2}\right)\\ &-\frac{\mu_{nf}\varepsilon^2}{\rho_{nf}K}u+\frac{F\varepsilon^2}{\sqrt{K}}u\sqrt{u^2+v^2}\,, \end{aligned} \tag{6}$$

$$\begin{aligned} u\frac{\partial v}{\partial x}+v\frac{\partial v}{\partial y}=&-\frac{\varepsilon^2}{\rho_{nf}}\frac{\partial p}{\partial y}+\frac{\varepsilon\mu_{nf}}{\rho_{nf}}\left(\frac{\partial^2 v}{\partial x^2}+\frac{\partial^2 v}{\partial y^2}\right)\\ &-\frac{\mu_{nf}\varepsilon^2}{\rho_{nf}K}v+\frac{F\varepsilon^2}{\sqrt{K}}v\sqrt{u^2+v^2}+\frac{\varepsilon^2(\rho\beta)_{nf}}{\rho_{nf}}g\,(T-T_C)\,. \end{aligned} \tag{7}$$

Energy

$$u\frac{\partial T}{\partial x}+v\frac{\partial T}{\partial y}=\alpha_{\text{eff}}\left(\frac{\partial^2 T}{\partial x^2}+\frac{\partial^2 T}{\partial y^2}\right), \tag{8}$$

where ε is the porosity and K is the porous medium permeability, F is the inertia coefficient, α_{eff} is the effective thermal diffusivity of the porous medium. The inertia coefficient can be expressed mathematically by

$$F=\frac{1.75}{\sqrt{150\varepsilon^3}}, \tag{9}$$

while the effective thermal diffusivity of the porous layer is given by

$$\alpha_{\text{eff}}=\frac{\lambda_{\text{eff}}}{\rho C_P}. \tag{10}$$

The effective thermal conductivity of the porous layer is given by

$$\lambda_{\text{eff}}=\varepsilon\lambda_{nf}+(1-\varepsilon)\lambda_s, \tag{11}$$

where λ_s represents the porous medium thermal conductivity and λ_{nf} indicates the nanofluid thermal conductivity.

Effective physical properties of the nanofluid were applied in the form [39, 45]:

- nanofluid density

$$\rho_{nf}=(1-\phi)\rho_f+\phi\rho_p, \tag{12}$$

- nanofluid buoyancy coefficient

$$(\rho\beta)_{nf}=(1-\phi)(\rho\beta)_f+\phi(\rho\beta)_p, \tag{13}$$

- nanofluid heat capacitance

$$(\rho C_p)_{nf}=(1-\phi)(\rho C_P)_f+\phi(\rho C_P)_S, \tag{14}$$

- nanofluid thermal conductivity

$$\frac{\lambda_{nf}}{\lambda_f}=\frac{\lambda_p+2\lambda_f-2\phi\left(\lambda_f-\lambda_p\right)}{\lambda_p+2\lambda_f+\phi\left(\lambda_f-\lambda_p\right)}, \tag{15}$$

- thermal diffusivity

$$\alpha_{nf}=\frac{\lambda_{nf}}{(\rho C_P)_{nf}}, \tag{16}$$

- nanofluid viscosity (Brinkman [54])

$$\mu_{nf} = \frac{\mu_f}{(1-\phi)^{2.5}}\,. \tag{17}$$

The above equations were written in a non-dimensional form using the following variables:

$$\begin{aligned} X &= \frac{x}{L}\,, \quad Y = \frac{y}{L}\,, \qquad U = \frac{u}{V_c}\,, \\ V &= \frac{v}{V_c}\,, \quad \theta = \frac{T-T_c}{T_h-T_c}\,, \quad P = \frac{p}{\rho V_c^2}\,. \end{aligned} \tag{18}$$

For the nanofluid layer:

$$\frac{\partial U}{\partial X} + \frac{\partial V}{\partial Y} = 0, \tag{19}$$

$$U\frac{\partial U}{\partial X} + V\frac{\partial U}{\partial Y} = -\frac{\partial P}{\partial X} + \frac{1}{\mathrm{Re}}\frac{\mu_{nf}\rho_f}{\mu_f\rho_{nf}}\left(\frac{\partial^2 U}{\partial X^2} + \frac{\partial^2 U}{\partial Y^2}\right), \tag{20}$$

$$\begin{aligned} U\frac{\partial V}{\partial X} + V\frac{\partial V}{\partial Y} = &-\frac{\partial P}{\partial Y} \\ &+ \frac{1}{\mathrm{Re}}\frac{\mu_{nf}\rho_f}{\mu_f\rho_{nf}}\left(\frac{\partial^2 V}{\partial X^2} + \frac{\partial^2 V}{\partial Y^2}\right)\frac{\rho_{nf}\beta_{nf}}{\rho_{nf}\beta_f}\frac{\mathrm{Gr}}{\mathrm{Re}^2}\theta, \end{aligned} \tag{21}$$

$$U\frac{\partial \theta}{\partial X} + V\frac{\partial \theta}{\partial Y} = \frac{\alpha_{nf}}{\alpha_f}\frac{1}{\mathrm{Re}\,\mathrm{Pr}}\left(\frac{\partial^2 \theta}{\partial X^2} + \frac{\partial^2 \theta}{\partial Y^2}\right). \tag{22}$$

For the porous layer:

$$\frac{\partial U}{\partial X} + \frac{\partial V}{\partial Y} = 0, \tag{23}$$

$$\begin{aligned} U\frac{\partial U}{\partial X} + V\frac{\partial U}{\partial Y} = &-\varepsilon^2\frac{\partial P}{\partial X} + \frac{\varepsilon}{\mathrm{Re}}\frac{\mu_{nf}\rho_f}{\mu_{nf}\rho_{nf}}\left(\frac{\partial^2 U}{\partial X^2} + \frac{\partial^2 U}{\partial Y^2}\right) \\ &- \frac{\varepsilon^2}{\mathrm{ReDa}}\frac{\rho_f}{\rho_{nf}}\frac{\mu_{nf}}{\mu_f}U + \frac{F\varepsilon^2}{\sqrt{\mathrm{Da}}}U\sqrt{U^2+V^2}\,, \end{aligned} \tag{24}$$

$$\begin{aligned} U\frac{\partial V}{\partial X} + V\frac{\partial V}{\partial Y} = &-\varepsilon^2\frac{\partial P}{\partial Y} + \frac{\varepsilon}{\mathrm{Re}}\frac{\mu_{nf}\rho_f}{\mu_f\rho_{nf}}\left(\frac{\partial^2 V}{\partial X^2} + \frac{\partial^2 V}{\partial Y^2}\right) \\ &- \frac{\varepsilon^2}{\mathrm{ReDa}}\frac{\rho_f}{\rho_{nf}}\frac{\mu_{nf}}{\mu_f}V + \frac{F\varepsilon^2}{\mathrm{Re}\sqrt{\mathrm{Da}}}V\sqrt{U^2+V^2}\,, \end{aligned} \tag{25}$$

$$U\frac{\partial \theta}{\partial X} + V\frac{\partial \theta}{\partial Y} = \frac{a_{\mathrm{eff}}}{a_f}\frac{1}{\mathrm{Re}\,\mathrm{Pr}}\left(\frac{\partial^2 \theta}{\partial X^2} + \frac{\partial^2 \theta}{\partial Y^2}\right). \tag{26}$$

Dimensionless boundary conditions are expressed as follows:

- at the inlet port:

$$U = 0, \quad V = 1, \quad \theta = 0; \tag{27}$$

- at the outlet port:

$$U = 0, \quad V = 0, \quad \frac{\partial U}{\partial X} = \frac{\partial \theta}{\partial X} = 0; \tag{28}$$

- at the walls:

$$U = 0, \quad V = 0, \quad \frac{\partial \theta}{\partial n} = 0; \tag{29}$$

- at the heated source:

$$U = 0, \quad V = 0, \quad \theta = 1. \tag{30}$$

Taking the same dynamic viscosity ($\mu_p = \mu_{nf}$) in both layers, interface boundary conditions are obtained by equating the tangential and normal velocities, shear and normal stresses, temperatures, and heat flow across the interface. Therefore, interface conditions can be expressed as:

$$\begin{aligned} \theta_p &= \theta_{nf}\,, \quad & \lambda_p \frac{\partial \theta_p}{\partial Y} &= \lambda_{nf} \frac{\partial \theta_{nf}}{\partial Y}\,, \\ U_p &= U_{nf}\,, \quad & \frac{\partial U_p}{\partial Y} &= \frac{\partial U_{nf}}{\partial Y}\,, \\ V_p &= V_{nf}\,, \quad & \frac{\partial V_P}{\partial Y} &= \frac{\partial V_{nf}}{\partial Y}\,. \end{aligned} \tag{31}$$

The local Nusselt number (Nu) along the heat source and the average Nusselt number can be defined as follows:

$$\begin{aligned} \mathrm{Nu} &= -\frac{\varepsilon \lambda_{nf} + (1-\varepsilon)\lambda_s}{\varepsilon \lambda_f + (1-\varepsilon)\lambda_s} \left.\frac{\partial \theta}{\partial y}\right|_{y=0}\,, \\ \overline{\mathrm{Nu}} &= \int_{\frac{h}{2}}^{\frac{3h}{2}} \mathrm{Nu}\, dx. \end{aligned} \tag{32}$$

3 Numerical procedure and code validation

3.1 Numerical scheme

The governing coupled equations, Eqs. (1)–(8), with the boundary conditions, Eqs. (27)–(28), were solved with the finite volume method (FVM). The SIMPLE (semi-implicit method for pressure linked equations) algorithm was adopted for the pressure velocity coupling (Patankar [55]). The second order QUICK (quadratic upstream interpolation for convective kinematics) scheme was used to discretize the continuity, momentum and energy equations. The obtained discretized equations were solved using a Gauss-Seidel iteration technique. A convergence criterion for continuity, momentum and energy equations was defined as such that the residuals become lower than 10^{-6}. In this study, the computations were performed on a personal computer with an Intel Core i3 – 3.6 GHz processor. The typical CPU time is around 100 423 s for a productive run.

3.2 Grid dependency

The grid independence test was performed for the present formulation (see Fig. 1) at $\mathrm{Gr} = 10^4$, $\mathrm{Re} = 10$, $\phi = 0$, $\mathrm{Da} = 10^{-3}$, $\delta = 0.5$ and $\gamma = 0.2$. Six uniform grids were tested. Table 2 shows the effect of mesh resolution on the average Nusselt number along the heated source. Using this result, a uniform finer grid of 140×140 was found to meet the requirements of both the grid independency study and the computational time limits.

Table 2: Grid independence study for $\mathrm{Gr} = 10^4$, $\mathrm{Re} = 10$ and $\mathrm{Da} = 10^{-3}$

Grid size	60×60	80×80	100×100	120×120	140×140	160×160
Average Nusselt number	7.688	7.686	7.683	7.695	7.709	7.713

3.3 Code validation

Validation of this study was done for natural convection flow in a layered porous cavity filled with nanofluid, as investigated by Chamkha and Ismael [39], for $\mathrm{Da} = 10^{-5}$, Rayleigh number (Ra) of 10^5 and $\phi = 0$. Comparisons with streamlines and isotherms are shown in Fig. 2, respectively. Results are in very good agreement with the benchmark solution for the considered range of parameters.

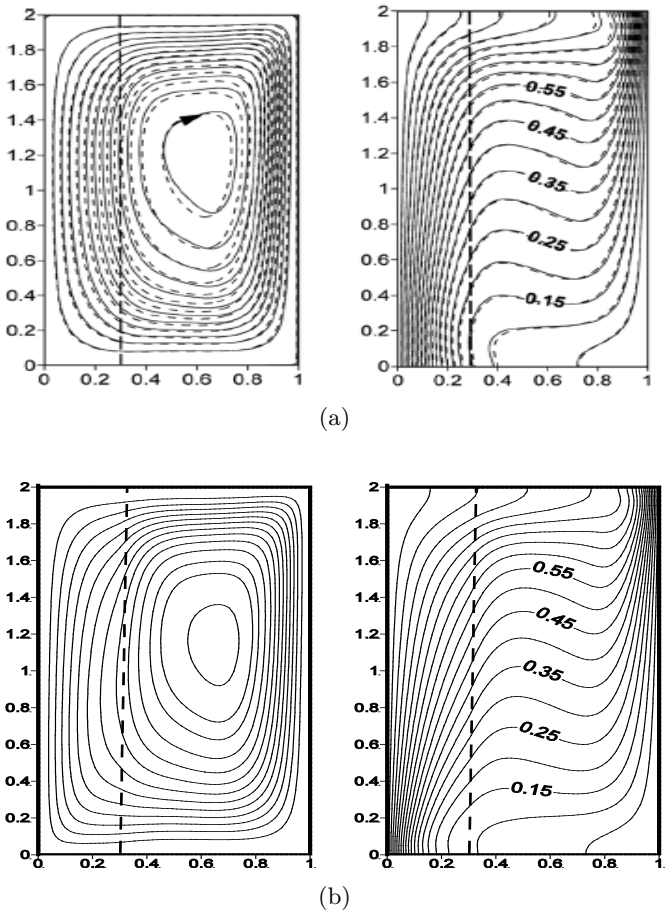

Figure 2: Comparison of streamlines and isotherms at Da $= 10^{-5}$ and Ra $= 10^5$: a) numerical results of Chamkha and Ismael [39], b) present study.

4 Results and discussion

This section presents numerical results for streamlines, isotherms and the average Nusselt number for various values of the Reynolds number ($1 \leq$ Re ≤ 1000), the Grashof number ($10^3 \leq$ Gr $\leq 10^6$), the Darcy number ($10^{-1} \leq$ Da $\leq 10^{-5}$), nanoparticles volume fraction ($0 \leq \phi \leq 0.06$), different nanoparticles (Fe_3O_4, Cu, Ag, Al_2O_3), thickness and position of porous layer ($0 \leq \gamma \leq 1$), ($0.1 \leq \delta \leq 0.9$), respectively. The porous layer porosity is fixed at $\varepsilon = 0.9$.

4.1 Effect of Reynolds and Grashof numbers

Figure 3 illustrates the effects of Reynolds and Grashof numbers on the structure of streamlines (top row) and isotherms (bottom row) at Da $= 10^{-3}$, $\phi = 0$, $\delta = 0.5$ and $\gamma = 0.2$. As can be seen from the figure, in the present study the Reynolds number characterizes the inlet vertical velocity of nanofluid at the inlet zone. Growth of this dimensionless parameter reflects more intensive penetration of nanofluid inside the cavity.

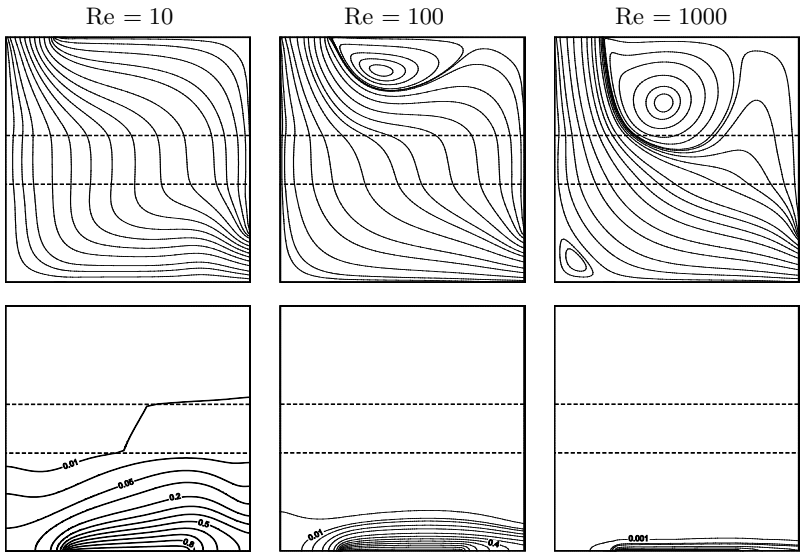

Figure 3: Streamlines (top) and isotherms (bottom) for different Reynolds numbers at Da $= 10^{-3}$, Gr $= 10^4$, $\phi = 0$, $\delta = 0.5$ and $\gamma = 0.2$.

At low Re $= 10$, flow is generally made up of a main (forced) flow, characterized by open streamlines, connecting the inlet and outlet of the cavity. However, near the porous layer, streamlines become vertical. This is due to the hydrodynamic resistance provided by the porous layer. An additional vortex is generated near the inlet port at the upper wall when Re is further increased to Re $= 100$. As the value of Reynolds number increases further (Re $= 1000$), the last vortex becomes stronger and a new small vortex appears in the left bottom corner, proving that the convection is more or less dependent on the intensity of the inflow.

On the other hand, isotherm lines for all values of Reynolds number are below the porous layer; cold nanofluid occupies entirely the cavity. For high Reynolds numbers, isotherms are clustered toward the bottom part of the

cavity. Due to inlet flow with high momentum, flow is entirely dominated by inertia forces.

The variation of the average Nusselt number on the heated plate with the Reynolds number for different Grashof numbers at $\phi = 0$, $\mathrm{Da} = 10^{-3}$, $\delta = 0.5$ and $\gamma = 0.2$ is shown in Fig. 4. Results indicate that the average Nusselt number enhances significantly with the increasing Reynolds and Grashof numbers, the increase of the latter leads to an improvement in the heat transfer rate. But, it is interesting to note that for $\mathrm{Re} = 100$, the average Nusselt number stays nearly the same with the increasing Grashof number.

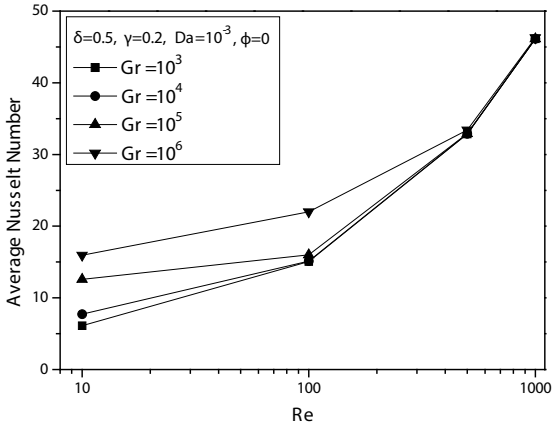

Figure 4: Variation of average Nusselt number with Reynolds number for different values of Grashof number at $\mathrm{Da} = 10^{-3}$, $\phi = 0$, $\delta = 0.5$ and $\gamma = 0.2$.

4.2 Effect of Darcy number

Figure 5 illustrates the distributions of streamlines and isotherms for different Darcy numbers (100, 10^{-2} and 10^{-5}) at $\mathrm{Gr} = 10^4$, $\mathrm{Re} = 100$, $\phi = 0.03$, $\delta = 0.5$, $\gamma = 0.2$ and Fe_3O_4. It can be seen from this figure that for a tiny Darcy number 10^{-5}, i.e., low permeability, flow is similar to the previous case of ($\mathrm{Da} = 10^{-3}$) and is characterized by open streamlines and a small vortex in the upper wall. The porous layer hinders fluid flow acting like a solid; streamlines are vertical in this section. Increasing Darcy number (10^{-2} and 100) means increasing the porous layer permeability and therefore, more cold nanofluid is allowed to penetrate the porous layer, considerably increasing the strength of the vortex. However, the Darcy number

variation does not have a significant effect on the distribution of isothermal lines, which are almost completely confined around the heated source, except for a slight rise of isotherms.

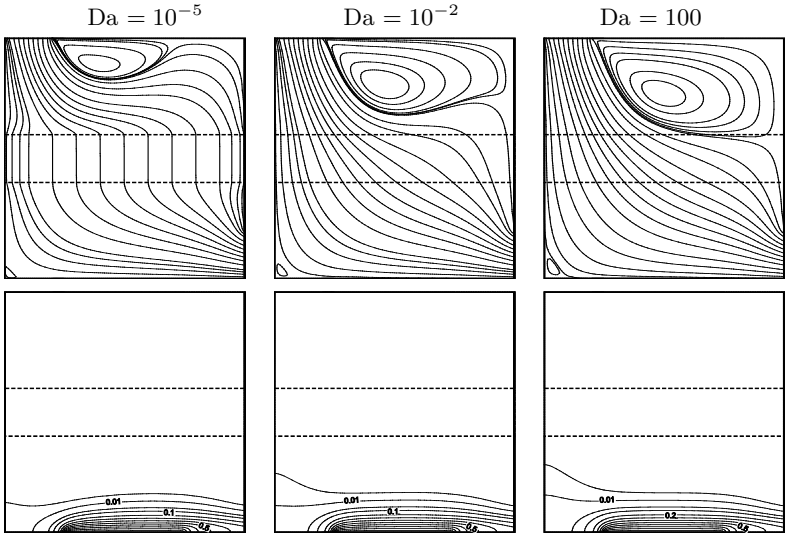

Figure 5: Streamlines (top) and isotherms (bottom) for different Darcy numbers at $\mathrm{Gr} = 10^4$, $\mathrm{Re} = 100$, $\phi = 0.03$, $\delta = 0.5$ and $\gamma = 0.2$ for Fe_3O_4.

Figures 6–7 show the overall heat transfer rate for different values of Darcy number, volume fraction of nanoparticle and Reynolds number with fixed

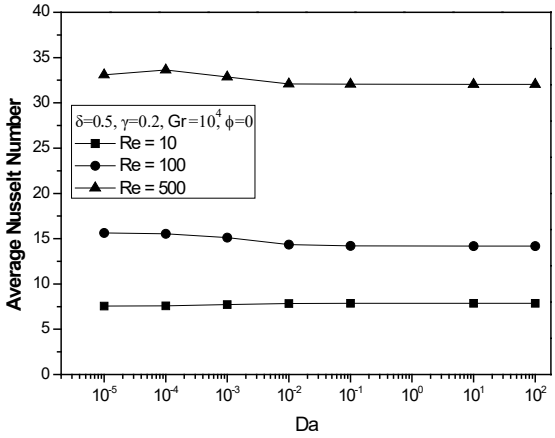

Figure 6: Variation of average Nusselt number with Darcy number for different values of Reynolds number at $\mathrm{Gr} = 10^4$, $\phi = 0$, $\delta = 0.5$ and $\gamma = 0.2$.

values of $Gr = 10^4$, $\delta = 0.5$ and $\gamma = 0.2$ for Fe_3O_4 nanoparticles. Similar to the previous case, an increase in the overall heat transfer rate is observed with the increasing Reynolds number for the fixed value of Darcy number. It can be seen, that for the fixed value of the Reynolds number, the Darcy number has not a significant effect on the average Nusselt number. The Darcy number effect is more clear in Fig. 7, where it demonstrates that the average Nusselt number is optimal at lower values of Darcy number ($Da = 10^{-5}$). On the other hand, the average Nusselt number increases with the increasing nanoparticles volume fraction for different Darcy numbers. In fact, the nanofluid thermal conductivity and heat transfer rate increase with the increasing nanoparticles volume fraction.

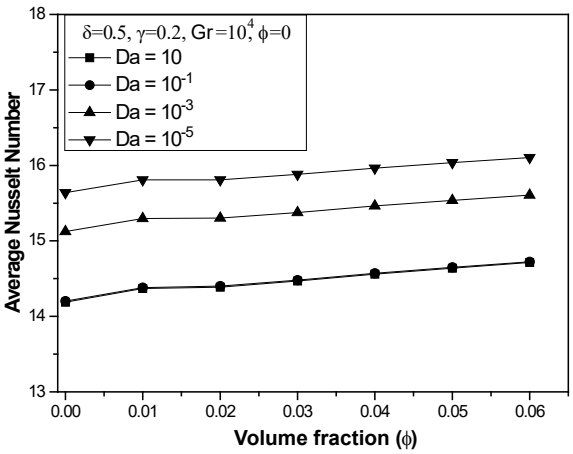

Figure 7: Variation of average Nusselt number with nanoparticles volume fractions for different values of Darcy number at $\gamma = 0.2$, $\delta = 0.5$, $Gr = 10^4$, $Re = 100$ for Fe_3O_4 nanoparticles.

4.3 Effect of nanoparticles type

Figure 8 shows streamline (top row) and isotherm (bottom row) profiles for three types of nanoparticles (Cu, Ag, Al_2O_3) in association with $Gr = 10^4$, $Da = 10^{-5}$, $Re = 10$, $\delta = 0.5$ and $\gamma = 0.2$. Therefore, a concentration of 4% has been chosen as a reference for each type of nanofluid. The flow structure is wired, connecting the inlet and outlet of the cavity and the isotherms are concentrated in the cavity lower part. It is noted that changing the type of nanoparticles has no discernible impact on the flow pattern and temperature distribution.

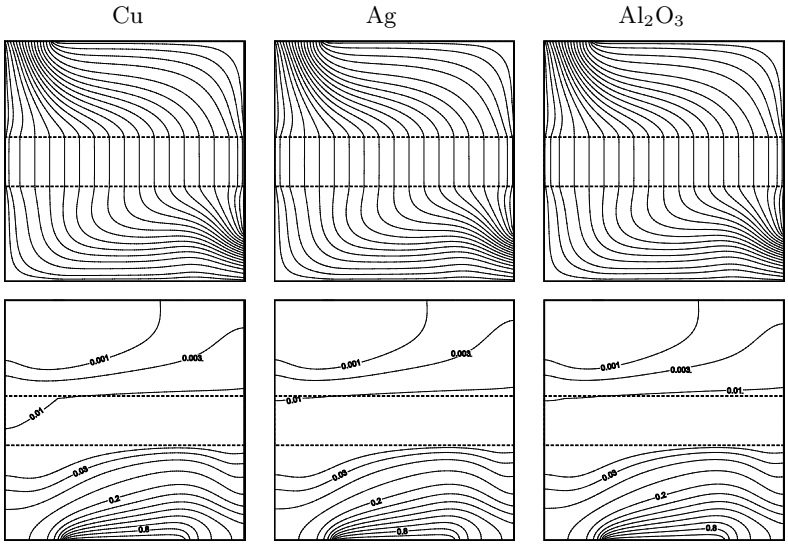

Figure 8: Streamlines (top) and isotherms (bottom) for different types of nanoparticles at Gr $= 10^4$, Re $= 10$, Da $= 10^{-5}$, $\phi = 0.04$, $\delta = 0.5$ and $\gamma = 0.2$.

The comparison of Nusselt number for various working nanofluids with various nanoparticles volume fractions for three different Darcy numbers and Gr $= 10^4$, Re $= 100$, $\gamma = 0.2$ and $\delta = 0.5$ is presented in Fig. 9. It is notable that Ag nanoparticles have the uppermost heat transfer rate chased by Cu, Fe_3O_4 and Al_2O_3 nanoparticles. This is due to the fact that Ag nanoparticle has a higher thermal conductivity compared to other nanoparticles. On the other hand, the Nusselt number increases with the

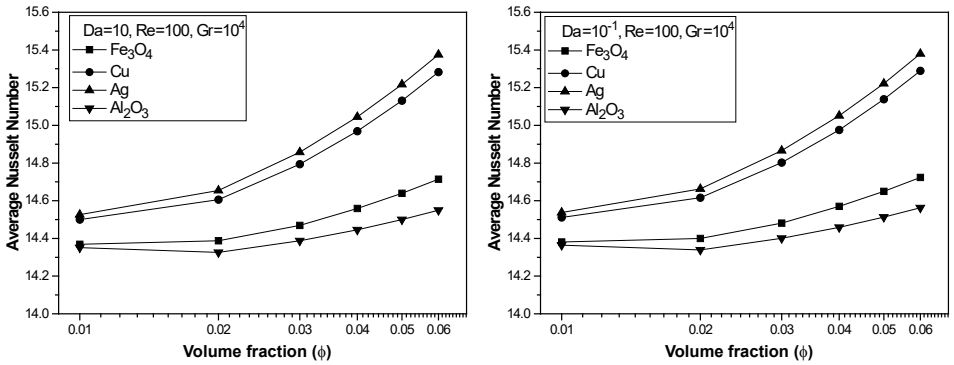

Figure 9: For caption see next page.

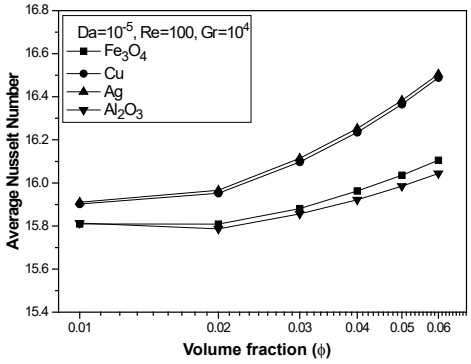

Figure 9: Variation of average Nusselt number with nanoparticles volume fractions for different types of nanoparticles and Darcy number at $\gamma = 0.2$, $\delta = 0.5$, $\mathrm{Gr} = 10^4$ and $\mathrm{Re} = 100$.

increasing volume fraction whatever the Darcy number and nanoparticle type.

4.4 Effect of porous layer thickness

Figure 10 illustrates the effects of porous layer thickness on streamline contour maps and isotherms, when $\mathrm{Da} = 10^{-3}$, $\mathrm{Re} = 100$, $\mathrm{Gr} = 10^4$ and $\phi = 0.04$ for Fe_3O_4 nanoparticles. It is observed that the change of porous layer thickness leads to significant changes in flow patterns. At $\gamma = 0$ (pure nanofluid), two vortices develop, a large one is located at the right top corner and a small vortex is located at the left bottom corner. As the value of γ increases, the size of circulating two cells gradually decreases. It should be noted that flow is directed toward the outlet port as the porous layer thickness increases. Corresponding isotherms are compressed near the heated source at the bottom wall, while all the upper part of the cavity is at a cold jet temperature, due to dominated forced convection. However, for a cavity completely filled by the porous medium ($\gamma = 1$) the through-flow fluid stream occupies the entire cavity and isotherm lines become wider and stratified due to strong effects of conduction larger than those of convection.

The behaviour of the average Nusselt number with γ is presented in Fig. 11. A growth of the porous layer size results in a rise of the heat transfer rate. This behaviour is imputed be to a reason that the effective thermal conductivity of the porous layer (Eq. (11)) is larger than that of the nanofluid layer.

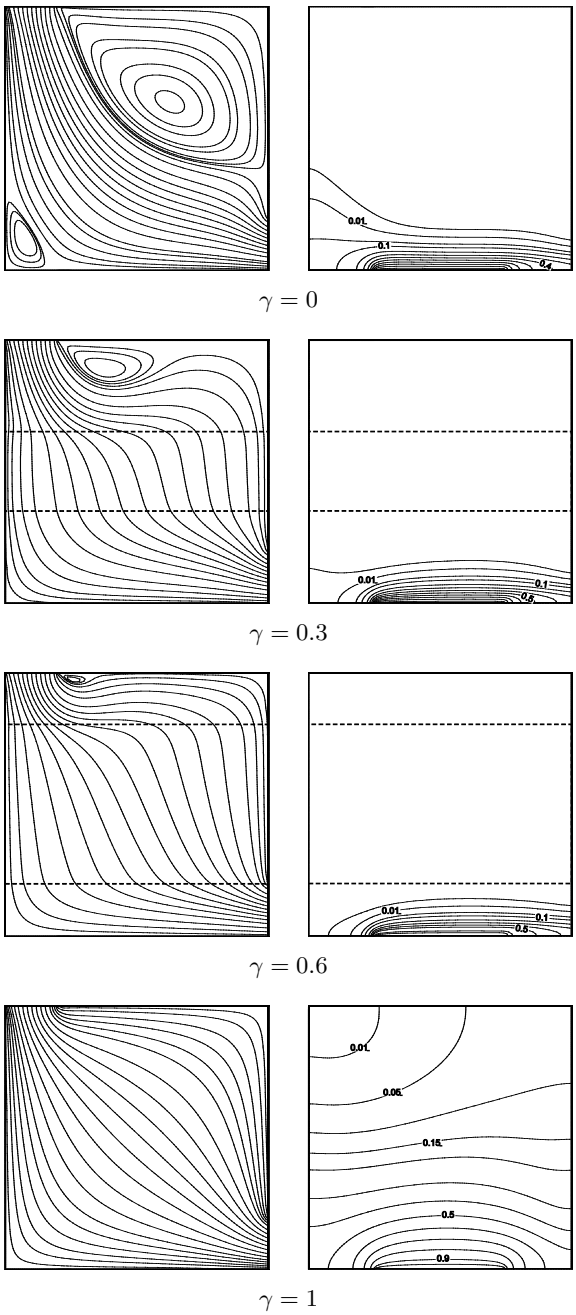

Figure 10: Streamlines (left) and isotherms (right) for different porous layer thicknesses (γ) at Gr $= 10^4$, Re $= 100$, Da $= 10^{-3}, \phi = 0.04$ for Fe_3O_4 nanoparticles.

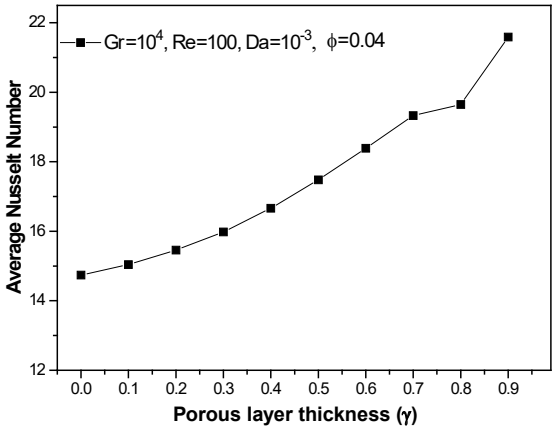

Figure 11: Variation of average Nusselt number with porous layer thickness for at $\mathrm{Gr} = 10^4$, $\mathrm{Re} = 100$, $\mathrm{Da} = 10^{-3}$ and $\phi = 0.04$ for Fe_3O_4 nanoparticles.

4.5 Effect of porous layer position

Figure 12 shows the distribution of streamlines (left row) and isothermal lines (right row) for various porous layer locations ($\delta = 0.1$, 0.3, 0.7 and 0.9) in the cavity for $\gamma = 0.2$, $\mathrm{Da} = 10^{-3}$, $\mathrm{Re} = 100$, $\mathrm{Gr} = 10^4$ and $\phi = 0.04$ for Fe_3O_4 nanoparticles. When the porous layer is located at the top wall ($\delta = 0.9$), two vortices appear in the right top corner and in the left bottom corner. However, for the case $\delta = 0.7$, cells disappear leaving a space for the main flow stream. Gradually as the porous layer approaches the bottom wall, two vortices reappear and become stronger, due to the dominance of convection flow. Isotherms are compressed at the cavity lower part as $\delta \leq 0.9$. It is noticed that when the heater source is surrounded by porous media ($\delta = 0.1$), isotherms ascend slightly, which means that the porous layer acts as a heat diffuser.

Figure 13 illustrates the average Nusselt number for the heated source at different aspect ratios (δ) and Darcy numbers. It is noted from the figure that the Nusselt number increases with the decreasing aspect ratio δ for all values of Darcy number. On the other hand, the Nusselt number is not much affected by a change in the Darcy number for $\delta \geq 0.5$, i.e., when the porous layer is far from the heated source. But usually, the Nusselt number increases with the decreasing Darcy number. In contrast, this tendency changes for the case $\delta = 0.1$, the heat transfer rate increases with the increasing Darcy number,which is due to the increase of effective thermal conductivity of the porous layer.

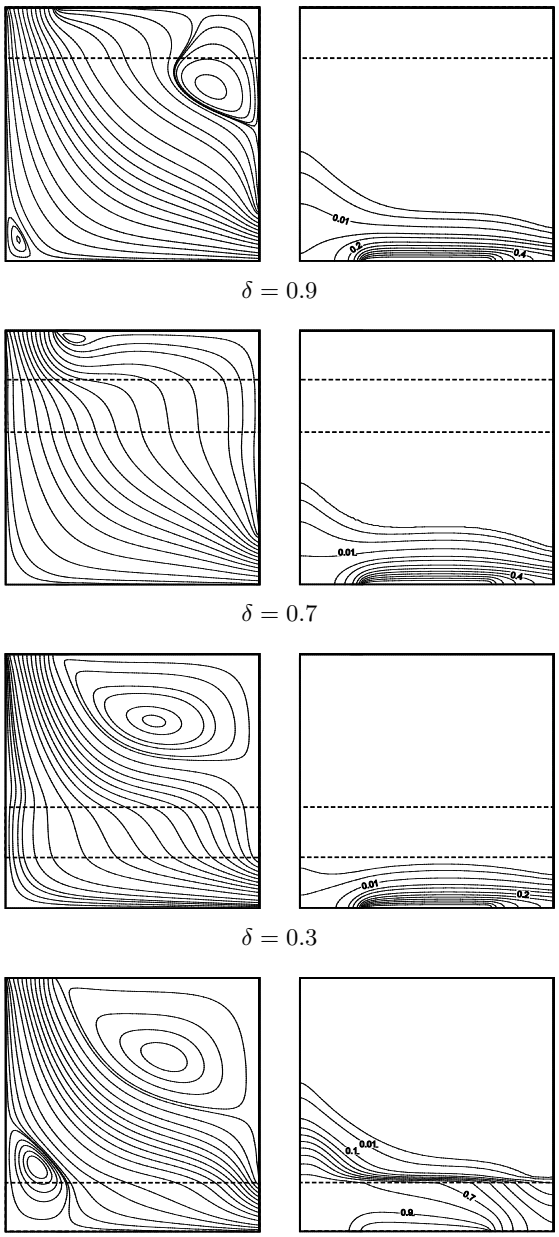

Figure 12: Streamlines (left) and isotherms (right) for different porous layer positions (δ) at Gr $= 10^4$, Re $= 100$, Da $= 10^{-3}$, $\gamma = 0.2$ and $\phi = 0.04$ for Fe_3O_4 nanoparticles.

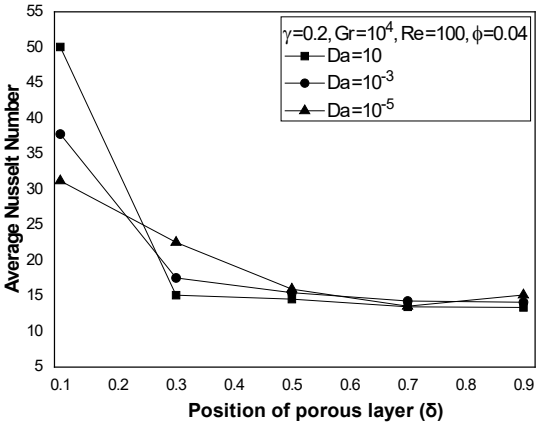

Figure 13: Variation of average Nusselt number with porous layer position at $\mathrm{Gr} = 10^4$, $\mathrm{Re} = 100$, $\mathrm{Da} = 10^{-3}$ and $\phi = 0.04$ for Fe_3O_4 nanoparticles.

5 Conclusions

The purpose of this work was to numerically analyze mixed convection in a vented square cavity filled with different nanofluids having a horizontal porous layer. The effects of governing parameters on flow and thermal fields characteristics were analyzed. A detailed analysis of streamlines distribution, isotherms and the average Nusselt number in the cavity were carried out to investigate the effect of Reynolds, Grashof and Darcy numbers, nanoparticle volume fraction, thickness and positions of porous layer on fluid flow and heat transfer in the mentioned cavity. The numerical results reported lead us to the following conclusions:

1. The average Nusselt number increases with the increasing volume fraction of nanoparticles, Reynolds and Grashof numbers for all studied Darcy numbers.

2. The flow pattern does not change substantially with the volume fraction and nanoparticles type.

3. The average Nusselt number is optimal at lower values of Darcy number.

4. An addition of nanoparticles to basic fluid leads to an increase of the average Nusselt number.

5. Ag nanoparticles seem to produce the highest values of Nusselt number compared to other types of nanoparticles.

6. A growth of the porous layer size increases the heat transfer rate and the position of the porous layer at the bottom wall has an uppermost effect on the heat transfer rate.

These various results should be useful for the design and optimization of several thermal engineering problems associated with heat exchangers. Subsequently, it would be interesting to complete this initiative by continuing the analysis and exploring the impact of discrete source location and three-dimensionality on the flow and heat transfer when the governing parameters are changed.

Received 12 October 2022

References

[1] Selvakumar R.D., Zhonglin D., Wu J.: *Heat transfer intensification by EHD conduction pumping for electronic cooling applications.* Int. J. Heat Fluid Flow **95**(2022), 108972.

[2] Ren F., Du J., Cai Y., Xu Z., Zhang D., Liu Y.: *Numerical simulation study on thermal performance of sub-tropical double-layer energy storage floor combined with ceiling energy storage radiant air conditioning.* Case Stud. Therm. Eng. **28**(2021), 101696.

[3] Niemann P., Schmitz G.: *Air conditioning system with enthalpy recovery for space heating and air humidification: An experimental and numerical investigation.* Energy **213**(2020), 118789.

[4] Dawar A., Wakif A., Thumma T., Shah N.A.: *Towards a new MHD non-homogeneous convective nanofluid flow model for simulating a rotating inclined thin layer of sodium alginate-based iron oxide exposed to incident solar energy.* Int. Commun. Heat Mass Transf. **130**(2022), 105800.

[5] Hongtao L., Zhang S., Ji Y., Sun M., Li X., Sheng Y.: *The influence of catchment scale on comprehensive heat transfer performance about tube fin heat exchanger in numerical calculation.* Energ. Rep. **8**(2022), 147–155.

[6] Raja M.A.Z., Shoaib M., Zubair G., Khan M.I., Gowda R.J.P., Prasannakumara B.C., Guedri K.: *Intelligent neuro-computing for entropy generated Darcy-Forchheimer mixed convective fluid flow.* Math. Comput. Simul. **201**(2022), 193–214.

[7] Awan A.U., Ahammad N.A., Ali B., Tag-ElDin E.M., Guedri K., Gamaoun F.: *Significance of thermal phenomena and mechanisms of heat transfer through the dynamics of second-grade micropolar nanofluids.* Sustainability **14**(2022), 9361.

[8] Mehrizi A.A., Farhadi M., Hassanzade Afroozi H., Sedighi K., Darz A.A.R.: *Mixed convection heat transfer in a ventilated cavity with hot obstacle: Effect of nanofluid and outlet port location*. Int. Commun. Heat Mass Transf. **39**(2012), 1000–1008.

[9] Ismael M.A., Jasim H.F.: *Role of the fluid-structure interaction in mixed convection in a vented cavity*. Int. J. Mech. Sci. **135**(2018), 190–202.

[10] Benzema M., Benkahla Y.Kh., Labsi N., Ouyahia S., El Ganaoui M.: *Second law analysis of MHD mixed convection heat transfer in a vented irregular cavity filled with Ag-MgO/water hybrid nanofluid*. J. Therm. Anal. Calorim. **137**(2019), 1113–1132.

[11] Selimefendigil F., Öztop H.F.: *Magnetohydrodynamics forced convection of nanofluid in multi-layered U-shaped vented cavity with a porous region considering wall corrugation effects*. Int. Commun. Heat Mass Transf. **113**(2020), 104551.

[12] Ataei-Dadavi I., Chakkingal M., Kenjeres S., Kleijn C.R., Tummers M.J.: *Experiments on mixed convection in a vented differentially side-heated cavity filled with a coarse porous medium*. Int. J. Heat Mass Transf. **149**(2020), 119238.

[13] Dhahad H.A., Al-Sumaily G.F., Alawee W.H., Thompson M.C.: *Aiding and opposing re-circulating mixed convection flows in a square vented enclosure*. Therm. Sci. Eng. Progress **19**(2020), 100577.

[14] Moayedi H.: *Investigation of heat transfer enhancement of Cu-water nanofluid by different configurations of double rotating cylinders in a vented cavity with different inlet and outlet ports*. Int. Commun. Heat Mass Transf. **126**(2021), 105432.

[15] Velkennedy R., Nisrin J.J., Kalidasan K., Rajeshkanna P.: *Numerical investigation of convective heat transfer in a rectangular vented cavity with two outlets and cold partitions*. Int. Commun. Heat Mass Transf. **129**(2021), 105659.

[16] Jamshed W., Eid M.R., Hussain S.M., Abderrahmane A., Safdar R., Younis O., Pasha A.A.: *Physical specifications of MHD mixed convective of Ostwald-de Waele nanofluids in a vented-cavity with inner elliptic cylinder*. Int. Commun. Heat Mass Transf. **134**(2022), 106038.

[17] Benos L., Sarris I.E.: *Analytical study of the magnetohydrodynamic natural convection of a nanofluid filled horizontal shallow cavity with internal heat generation*. Int. J. Heat Mass Transf. **130**(2019), 862–873.

[18] Arani A.A.A., Mahmoodi M., Amini M.: *Free convection in a nanofluid filled square cavity with a horizontal heated plate*. Defect Diffus. Forum **312-315**(2011), 433–438.

[19] Selimefendigil F., Öztop H.F.: *Mixed convection of ferrofluids in a lid driven cavity with two rotating cylinders*. Eng. Sci. Techn. Int. J. **18**(2015), 439–451.

[20] Rabbi Kh.Md., Saha S., Mojumder S., Rahman M.M., Saidur R., Ibrahim T.A.: *Numerical investigation of pure mixed convection in a ferrofluid-filled lid-driven cavity for different heater configuration*. Alexandria Eng. J. **55**(2016), 127–139.

[21] Elshehabey H.M., Raizah Z., Öztop H.F., Ahmed S.E.: *MHD natural convective flow of Fe_3O_4-H_2O ferrofluids in an inclined partial open complex-wavy-walls ringed enclosures using non-linear Boussinesq approximation*. Int. J. Mech. Sci. **170**(2020), 105352.

[22] Jakeer S., Reddy P.B.A., Rashad A.M., Nabwey H.A.: *Impact of heated obstacle position on magneto-hybrid nanofluid flow in a lid-driven porous cavity with Cattaneo-Christov heat flux pattern.* Alexandria Eng. J. **60**(2021), 821–835.

[23] Wang A., Xu H.: *Highly accurate wavelet-homotopy solutions for mixed convection hybrid nanofluid flow in an inclined square lid-driven cavity.* Comput. Math. Appl. **108**(2022), 88–108.

[24] Jayaprakash M.C., Alsulami M.D., Shanker B., Kuma R.S.V. *Investigation of Arrhenius activation energy and convective heat transfer efficiency in radiative hybrid nanofluid flow.* Waves Random Complex Media (2022), 1–13.

[25] Dutta S., Bhattacharyya S., Pop I.: *Effect of hybrid nanoparticles on conjugate mixed convection of a viscoplastic fluid in a ventilated enclosure with wall mounted heated block.* Alexandria Eng. J. **62**(2023), 99–111.

[26] Neild D.A., Bejan A.: *Convection in Porous Media.* (3rd Edn.). Springer-Verlag, 2006.

[27] Balla C. S., Kishan N., Gorla R.S.R, Gireesha B.J.: *MHD boundary layer flow and heat transfer in an inclined porous square cavity filled with nanofluids.* Ain Shams Eng. J. **8**(2017), 237–254.

[28] Malik S., Nayak A.K.: *MHD convection and entropy generation of nanofluid in a porous enclosure with sinusoidal heating.* Int. J. Heat Mass Transf. **111**(2017), 329–345.

[29] Sheremet M.A., Roşca N.C., Roşca A.V., Pop I.: *Mixed convection heat transfer in a square porous cavity filled with a nanofluid with suction/injection effect.* Comput. Math. Appl. **76**(2018), 2665–2677.

[30] Abu-Hamdeh N.H., Öztop H.F., Alnefaie K.A.: *A computational study on mixed convection in a porous media filled and partially heated lid-driven cavity with an open side.* Alexandria Eng. J. **59**(2020), 1735–1750.

[31] Mabood F., Yusuf T.A., Sarris I.E.: *Entropy generation and irreversibility analysis on free convective unsteady MHD Casson fluid flow over a stretching sheet with Soret/Dufour in porous media.* Spec. Top. Rev. Porous Media: Int. J. **11**(2020), 6, 595–611.

[32] Kumar R.N., Gowda R.J.P., Gireesha B.J., Prasannakumara B.C.: *Non-Newtonian hybrid nanofluid flow over vertically upward/downward moving rotating disk in a Darcy–Forchheimer porous medium.* Eur. Phys. J. Spec. Top. **230**(2021), 1227–1237.

[33] Kashyap D., Dass A.K.: *Influence of cavity inclination on mixed convection in a double-sided lid-driven cavity with a centrally inserted hot porous block.* Int. J. Therm. Sci. **181**(2022), 107732.

[34] Alsedais N., Aly A.M., Mansour M.A.: *Local thermal non-equilibrium condition on mixed convection of a nanofluid-filled undulating cavity containing obstacle and saturated by porous media.* Ain Shams Eng. J. **13**(2022), 101562.

[35] Choudhary P., Ray R.K.: *MHD natural convective flow in a porous corrugated enclosure: Effects of different key parameters and discrete heat sources.* Int. J. Therm. Sci. **181**(2022), 107730.

[36] Nammi G., Deka D.K., Pati S., Baranyi L.: *Natural convection heat transfer within a square porous enclosure with four heated cylinders*. Case Stud. Therm. Eng. **30**(2022), 101733.

[37] Kumar V., Murthy S.V.S.S.N.V.G.K., Kumar B.V.R.: *Multi-force effect on fluid flow, heat and mass transfer, and entropy generation in a stratified fluid-saturated porous enclosure*. Math. Comput. Simul. **203**(2023), 328–367.

[38] Mercier J-F., Weisman C., Firdaouss M., Le Quéré P.: *Heat transfer associated to natural convection flow in a partly porous cavity*. J. Heat Transf. **124**(2002), 130–143.

[39] Chamkha A.J., Ismael M.A.: *Natural convection in differentially heated partially porous layered cavities filled with a nanofluid*. Numer. Heat Transf. A-Appl. **65**(2014), 1089–1113.

[40] Le Bars M., Worster M.G.: *Interfacial conditions between a pure fluid and a porous medium: implications for binary alloy solidification*. J. Fluid Mech. **550**(2006), 149–173.

[41] Carcadea E., Varlam M., Ismail M., Ingham D.B., Marinoiu A., Raceanu M., Jianu C., Patularu L., Ion-Ebrasu D.: *PEM fuel cell performance improvement through numerical optimization of the parameters of the porous layers*. Int. J. Hydrogen Energ. **45**(2020), 7968–7980.

[42] Aly A.M., Raizah Z.A.S., Ahmed S.E.: *mixed convection in a cavity saturated with wavy layer porous medium: Entropy generation*. J. Thermophys. Heat Transf. **32**(2018), 3, 764–780.

[43] Astanina M.S., Sheremet M.A., Oztop H.F., Abu-Hamdeh N.: *MHD natural convection and entropy generation of ferrofluid in an open trapezoidal cavity partially filled with a porous medium*. Int. J. Mech. Sci. **136**(2018), 493–502.

[44] Selimefendigil F., Öztop H.F.: *Thermal management and modeling of forced convection and entropy generation in a vented cavity by simultaneous use of a curved porous layer and magnetic field*. Entropy **23**(2021), 152.

[45] Gibanov N.S., Sheremet M.A., Öztop H.F., Abu-Hamdeh N.: *Effect of uniform inclined magnetic field on mixed convection in a lid-driven cavity having a horizontal porous layer saturated with a ferrofluid*. Int. J. Heat Mass Transf. **114**(2017), 1086–1097.

[46] Al-Srayyih B.M., Gao S., Hussain S.H.: *Natural convection flow of a hybrid nanofluid in a square enclosure partially filled with a porous medium using a thermal non-equilibrium model*. Phys. Fluids **31**(2019), 043609.

[47] Al-Zamily A.M.J.: *Analysis of natural convection and entropy generation in a cavity filled with multi-layers of porous medium and nanofluid with a heat generation*. Int. J. Heat Mass Transf. **106**(2017), 1218–1231.

[48] Moria H.: *Natural convection in an L-shape cavity equipped with heating blocks and porous layers*. Int. Commun. Heat Mass Transf. **126**(2021), 105375.

[49] Alsabery A.I., Hajjar A., Raizah Z.A.S., Ghalambaz M., Hashim I., Chamkha A.J.: *Impact of finite wavy wall thickness on entropy generation and natural convection of nanofluid in cavity partially filled with non-Darcy porous layer*. Neural Comput. Appl. **32**(2020), 13679–13699.

[50] Chordiya J.S., Sharma R.V.: *Numerical study on the effects of multiple internal diathermal obstructions on natural convection in a fluid-saturated porous enclosure*. Arch. Mech. Eng. **65**(2018), 4, 553–578.

[51] Rana G.C.: *The onset of thermal convection in couple-stress fluid in hydromagnetics saturating a porous medium*. Bull. Pol. Acad. Sci. Tech. Sci. **62**(2014), 2, 357–362.

[52] Saeed F., R., Al-Dulaimi M.A.: *Numerical investigation for convective heat transfer of nanofluid laminar flow inside a circular pipe by applying various models*. Arch. Thermodyn. **42**(2021), 1, 71–95.

[53] Korib K., Ihaddadene N., Bouakkaz R., Khelili Y.: *Numerical simulation of forced convection of nanofluid around a circular cylinder*. Arch. Thermdyn. **40**(2019), 2, 3–16

[54] Brinkman H.C.: *The viscosity of concentrated suspensions and solutions*. J. Chem. Phys. **20**(1952), 571–581.

[55] Patankar S.V.: *Numerical Heat Transfer and Fluid Flow*. Hemisphere, McGraw-Hill, Washington DC 1980.